Effect of substrate pre-treatment on the low cycle fatigue performance of tungsten carbide-cobalt coated additive manufactured 316 L substrates

Einfluss der Substratvorbehandlung auf das Kurzzeitermüdungsverhalten von Wolframkarbid-Kobalt beschichteten additiv gefertigten 316 L Substraten

W. Tillmann[1], L. Hagen[1], K.-U. Garthe[2], K.-P. Hoyer[2], M. Schaper[2]

Numerous studies already identified that the fatigue strength of 316 L parts processed by laser beam melting (LBM) is distinctly affected by the surface integrity. Among others, surface defects as well as residual stresses are of crucial importance. Despite new findings in the field of surface engineering of laser beam melting (LBM) parts, the low cycle fatigue strength of thermally sprayed additively manufactured substrates has not been in the focus of research to date. This study aims at evaluating the effect of different pre-treatments onto 316 L substrates processed by laser beam melting (LBM) prior to the deposition of a high velocity oxy-fuel (HVOF) sprayed tungsten carbide-cobalt coating and their effect on the low cycle fatigue strength. Therefore, 316 L substrates were examined in their as-built state as well as after grit blasting with regards to the surface roughness, strain hardening effects, and residual stresses. To differentiate between topographical effects and residual stress related phenomena, stress-relieved 316 L substrates served as reference throughout the investigations. The tungsten carbide-cobalt coated and differently pre-treated 316 L substrates were mechanically tested under quasi-static and dynamic load conditions. Besides the low cycle fatigue strength, the fracture toughness as well as the fracture mechanism were identified based on fracture surface analysis.

Keywords: Laser beam melting **/** high velocity oxy-fuel spraying **/** tungsten carbide-cobalt **/** 316 L **/** substrate pre-treatment

Schlüsselwörter: Laserstrahlschmelzen **/** Hochgeschwindigkeitsflammspritzen **/** Wolframkarbid-Kobalt **/** 316 L **/** Substratvorbehandlung

[1] TU Dortmund University, Institute of Materials Engineering, DORTMUND, FEDERAL REPUBLIC OF GERMANY
[2] Paderborn University, Chair of Materials Science, PADERBORN, FEDERAL REPUBLIC OF GERMANY

Corresponding author: L. Hagen, TU Dortmund University, Institute of Materials Engineering, DORTMUND, FEDERAL REPUBLIC OF GERMANY, E-Mail: leif.hagen@tu-dortmund.de

1 Introduction

Applying laser beam melting (LBM), the component is built up successively and layer-based [1]. Furthermore, it offers the possibility of the direct production of ready-to-use components and products from computer-aided design data and metal powders, thus eliminating the cost-intensive process steps of tool design and manufacturing [2]. In laser beam melting (LBM), an iterative process is carried out. First, the metal powder is applied as a layer on the building platform by a coater and then locally melted by a high-energy laser to achieve the required geometry of the respective layer. Once the powder layer has been processed, the building platform is lowered and the process starts again with the application of a new powder layer. Each new layer is connected to the previous one, so that the desired three-dimensional geometry is achieved. No further tools are required, since the laser paths and the geometry of the layers are generated solely from a prepared 3D computer-aided design data set [3]. Due to the inherent process characteristics, the produced samples still exhibit a varying residual porosity and a high surface roughness [4]. The resulting microstructural characteristics (e. g. grain orientation) and residual stresses, among others, depend on the thermal history during processing, which in turn is associated with the building strategy [5].

AISI 316 L stainless steel, known as 1.4404, is an iron-based alloy. The main alloying elements are chromium, nickel and molybdenum. Therefore, the material provides good mechanical properties and adequate corrosion resistance [6]. Moreover, the material shows a good weldability and is thus ideally suited for laser beam melting (LBM) [7]. Despite a remaining low porosity in additively manufactured 316 L steel, the produced material also possesses high strength and good ductility [8]. Nevertheless, compared to hard materials, 316 L steel provides a poor resistance against abrasion due to its low hardness.

Due to their outstanding properties, tungsten carbide-cobalt coatings evolved into a predominant coating system for wear protection over the last decades, which is typically employed at operating temperatures up to 400 °C [9, 10]. Commonly, tungsten carbide-cobalt coatings are deposited by using high velocity oxy-fuel (HVOF) spraying. Inherent process characteristics, such as high kinetic energy of the impinging spray particles, allow the application of dense coatings with a good adhesion to the substrate by mechanical interlocking effects of splats. The coatings microstructure (e. g. porosity level, amount of cracks and impurities, interconnection of the individual splats) constitutes the resulting mechanical properties. However, the mechanical properties of tungsten carbide-cobalt coatings primarily depend on the tungsten carbide particle size, the amount and distribution of tungsten carbide particles, the content of the cobalt binder phase and its mean free path [11]. For high velocity oxy-fuel (HVOF) sprayed tungsten carbide-cobalt coatings, tungsten carbide decomposition as well as the formation of eta carbides (e. g. M_6C, $M_{12}C$ etc., M = metal) are under certain aspects of significant technical importance as they are detrimental to mechanical behavior under quasi-static and dynamic load conditions.

Under practical operating conditions, components are usually subjected to mechanical-cycling loads. A sufficient fatigue strength of the composites (i. e. laser beam melting (LBM) substrate/high velocity oxy-fuel (HVOF) coating) is regarded as an essential criterion to ensure the functionality. The aim of the present research work is to postulate a correlation between the effect of different substrate surface conditions (i. e. grit blasted, as-built) and the low cycle fatigue strength of the produced tungsten carbide-cobalt coated 316 L substrate composites under quasi-static and dynamic load conditions. To differentiate between topographical effects and residual stress related phenomena, stress-relieved 316 L substrates served as reference throughout the investigations.

2 Experimental methods

2.1 Additively manufactured 316 L substrates

Dog-bone shaped low cycle fatigue samples were produced with a nominal gage length of 8 mm × 3 mm × 2.5 mm using the laser beam melting system SLM 250^{HL} (SLM Solutions, Germany). The samples were generated from a 316 L stainless steel powder (SLM Solutions, Germany). As obtained from laser diffraction analysis (Mastersizer 2000, Malvern Panalytical, Germany), the 50th percentile

in diameter (D50) of the volumetric particle size distribution was 32.0 μm (D10 = 16.2 μm, D90 = 57.8 μm). The samples were built applying the process parameters, *Table 1*.

All samples were manufactured under argon atmosphere to prevent oxygen uptake and oxidation phenomena. The building direction was vertical using the skin-core strategy. For the 316 L stainless steel powder (i.e. feedstock) and the 316 L laser beam melting (LBM) substrate, the chemical composition was verified by x-ray fluorescence analyses (Revierlabor, Germany), *Table 2*. As verified by x-ray microcomputed tomography (Xradia 520 Versa, Zeiss, Germany), the produced 316 L laser beam melting (LBM) substrates exhibit an overall porosity of approximately 0.16 % (measured with a voxel edge length of 70 nm).

2.2 Substrates pre-treatment and coating deposition

Prior to the coating deposition, the 316 L substrates were grit blasted using alumina with an abrasive particle size of F240 (according to the Federation of European Producers of Abrasives). Within this study, the sample type is referred to as F240. A 316 L substrate in its as-built condition served as a reference and is referred to as AB. To distinguish between topographical and mechanical causes (i.e. residual stresses) and their effect on the fatigue behavior of the laser beam melting (LBM) substrate/ high velocity oxy-fuel (HVOF) coating composite, a stress-relief heat treatment was conducted in a second measurement series. The stress-relief heat treatment was executed at 650 °C with a heating rate of 5.4 °C min^{-1} and a holding time of 120 min, using a high temperature vacuum oven (U 80/1H, Schmetz, Germany) [12]. The process as well as the subsequent furnace cooling was carried out in vacuum. The corresponding sample types are referred to as F240_SRT, and AB_SRT, respectively.

For the coating deposition, a high velocity oxy-fuel (HVOF) WokaJet 400 spraying system (Oerlikon Metco, Switzerland) equipped with an Oerlikon Metco MultiCoat controller system, and a Twin-120-H powder feeder were used. An agglomerated and sintered tungsten carbide-cobalt powder (Woka 3102, Oerlikon Metco, Switzerland) with 88 weight % of tungsten carbide and 12 weight % of cobalt served as feedstock. The spray torch was mounted on an ABB IRB 4600 60/2.05 6-axis robot. The spraying experiments were carried out on a turning lathe. To achieve an all-side coating, the different pre-treated 316 L substrates were rotated using a rotating velocity of 600 min^{-1}. A transverse speed of 130 mm s^{-1} was applied for moving the spray torch over the sample. Each coating was conducted with a front side cooling (i.e. pipeline with straight outlet openings; inside diameter: 7.7 mm) using compressed air with a maximum flow velocity of 154 m/s ±2 m/s (as verified by differential pressure measurements, pitot tube AFLPS 588701, differential pressure transmitter DKP1010, Driesen

Table 1. Selective laser melting (SLM) process parameters used in this study.

Process parameter	Local strategy	
	Volume contour	Volume area
Laser power [W]	100	175
Laser scanning speed [mm s^{-1}]	565	750
Hatch distance [mm]	–	0.12
Layer thickness [μm]	30	30

Table 2. Comparison of the chemical composition for the 316 L feedstock and the 316 L laser beam melting (LBM) substrate.

Sample	O	Al	Si	Ti	Cr	Mn	Fe	Co	Ni	Cu	Mo	others
SLM substrate	0.07	0.11	0.51	0.05	17.1	1.00	bal.	0.05	11.5	0.12	2.29	< 0.03
Feedstock	0.045	0.05	0.78	0.03	16.9	1.40	bal.	0.03	11.5	0.04	2.39	< 0.03

in weight %

+Kern, Germany). The spray parameter settings were kept constant for all experiments, *Table 3*.

2.3 Analytic methods

Prior to the coating deposition, the 316 L substrate surfaces were examined using the 3D surface measurement system Infinite Focus (Alicona, Austria). The mean roughness R_a and mean roughness depth R_z were obtained from the reconstructed surfaces. X-ray diffraction analysis were conducted at the 316 L substrate surfaces as well as the tungsten carbide-cobalt coating surfaces (i.e. of the laser beam melting (LBM) substrate/high velocity oxy-fuel (HVOF) coating composites) using a Bruker Advanced D8 diffractometer (Bruker, Massachusetts, U.S.) with chromium K-alpha ($\lambda = 0.22910$ nm) and copper K-alpha ($\lambda = 0.15406$ nm) radiation to determine the phase composition and the residual stresses. With regard to the residual stress measurement, the $\sin^2\psi$ method was employed [13]. For the 316 L substrates, the austenitic γ-phase (220) reflection in an angular range of $2\theta = 126.5–131°$ was examined. In contrast, the hexagonal tungsten mono-carbide (201) reflection in an angular range of $2\theta = 83–85.5°$ was taken into account for the tungsten carbide-cobalt coating surfaces. For both stress measurements, the step width and exposure time were respectively 0.1° and 2.5 s for each step. The measurements were performed for various tilt angles $\psi = \pm$ (0; 7; 14; 21; 28; 35; 42; 49), and rotation angles $\phi = \pm$ (0; 180). The d–ψ data was analyzed using the software Leptos (Bruker, Massachusetts, U.S.). For the austenitic γ-phase (220) reflection, a Young's modulus, E, of 207 GPa and a Poisson ratio, v, of 0.28 were used [14]. The x-ray elastic constants ($s_1 = -1.36E–6$ mm^2 N^{-1}; $\frac{1}{2}$ $s_2 = 6.19E–6$ mm^2 N^{-1}) were computed based on the Voigt model [13]. As opposed to that, a value of 515 GPa and 0.19 for the Young's modulus and

the Poisson ratio was used to calculate the residual stress with regard to the hexagonal tungsten mono-carbide (201) reflection [14]. In this respect, the x-ray elastic constants were $s_1 = -0.37E–6$ mm^2 N^{-1}, and $\frac{1}{2}$ $s_2 = 2.31E–6$ mm^2 N^{-1}. To evaluate an all-side coating, representative samples (i.e. laser beam melting (LBM) substrate/high velocity oxy-fuel (HVOF) coating composites) were investigated prior to the low cycle fatigue tests by means of cross-section analysis using the optical microscope BX51M (Olympus, Japan). Simultaneously, the coating microstructure and its bonding to the substrate were examined in order to preclude premature failures (e.g. coating delamination). To assess the introduction of strain hardening effects by impinging grit-blasting particles during substrate preparation, the hardness was determined at the cross section of the laser beam melting (LBM) substrate/high velocity oxy-fuel (HVOF) coating composites. The hardness was measured at the substrate-coating interface by means of load and displacement sensing curves using the nanoindentor G200 (Agilent Technology, USA) [15]. The indents were performed parallel to the substrate-coating interface in regular intervals. Vickers indention experiments were conducted at the cross-section to determine the fracture toughness K_{IC} of the tungsten carbide-cobalt coating. A load of 49 N was applied using the universal hardness tester DIA-TESTOR 7521 (Wolpert, Germany). The length of the microcracks (Palmquist cracks), generated at the corners of the indention, was measured via cross-section images and the K_{IC} value was calculated according to the equation by Shetty and Wright [16].

2.4 Low cycle fatigue tests

The low cycle fatigue tests were performed on a servo-hydraulic testing machine (MTS 858 Table Top System, MTS Systems Corporation, Minneso-

Table 3. Spray parameter settings.

Oxygen flow [SLPM]	876	Powder carrier gas [SLPM]	2×4.6
Kerosene flow [SLPH]	23	Feeding disc setting [%]	20
Spray distance [mm]	300	Stirrer setting [%]	50
Overruns	20		

ta). The different laser beam melting (LBM) substrate/high velocity oxy-fuel (HVOF) coating composites were fatigued in strain-controlled tests at total strain amplitudes of 0.35 %, 0.50 % and 0.80 %. The low cycle fatigue tests were performed at room temperature with an R-ratio of -1 and a strain rate of $6 \times 10^{-3}\,\mathrm{s}^{-1}$. An extensometer was used to determine the exact strain. With the results generated here, it is possible to estimate the service life as well as the hardening and softening behavior under dynamic stress based on the cyclic stress-strain curve (hysteresis curve). After testing, the microstructural appearance and failure mechanism were analyzed at the fractured surfaces using a digital microscope (Leica DVM6, Leica Microsystems, Germany). To assess the formation of fatigue cracks, longitudinal-sections in building direction of the samples (perpendicular to the crack formation) were metallographically prepared and afterwards examined by using the optical microscope BX51M (Olympus, Japan).

3 Results and discussion

Regarding the surface roughness of the differently pre-treated 316 L substrates, it is found that the substrate in its as-built state (sample AB) exhibits a mean roughness Ra of $9.8\,\mu\mathrm{m} \pm 1.0\,\mu\mathrm{m}$ and a mean roughness depth R_z of $63.2\,\mu\mathrm{m} \pm 5.8\,\mu\mathrm{m}$, *Table 4*. In contrast, the grit blasted substrate (sample F240) possesses a mean roughness R_a of $7.3\,\mu\mathrm{m} \pm 0.4\,\mu\mathrm{m}$, whereas the mean roughness depth R_z was $43.5\,\mu\mathrm{m} \pm 3.0\,\mu\mathrm{m}$. For the heat-treated samples, the 3D surface measurement indicates a similar surface roughness, Table 4. Accordingly, sample AB_SRT

shows a mean roughness R_a of $9.9\,\mu\mathrm{m} \pm 2.1\,\mu\mathrm{m}$ and mean roughness depth R_z of $66.1\,\mu\mathrm{m} \pm 15.7\,\mu\mathrm{m}$, whereby sample F240_SRT features a mean roughness R_a of $7.8\,\mu\mathrm{m} \pm 1.8\,\mu\mathrm{m}$ and mean roughness depth R_z of $45.3\,\mu\mathrm{m} \pm 11.1\,\mu\mathrm{m}$.

X-ray diffraction analyses reveal that the differently pre-treated 316 L substrates (sample AB, AB_SRT, F240, and F240_SRT) mainly consist of a face-centred cubic, austenitic phase (γ-phase) with a preferred grain orientation in the (111) direction, *Figure 1*a. The feedstock (x-ray diffraction data not shown) is mainly composed of the γ-phase with some minor content of the body-centred cubic, ferritic phase. It is assumed that the ferritic phase partially converted into the γ-phase by remelting during laser beam melting (LBM). Some small amounts of the ferritic phase remain in the microstructure. When compared to the non-heat-treated substrates (sample AB, and F240), the x-ray diffraction patterns obtained from the heat-treated substrates (sample AB_SRT, and F240_SRT) indicate the absence of phase transformation processes within the experimental resolution. Nevertheless, the x-ray diffraction pattern for sample F240 demonstrates a peak broadening for the (111), (200) and (220) reflections, which can be presumably attributed to (i) the introduction of microstresses or (ii) grain refinement effects due to defects in the lattice structure. In contrast, the grit blasted and additional heat-treated substrate (i.e. sample F240_SRT) shows a reduction in the full width at half maximum of the peak reflections, suggesting a reduction in microstresses or a change in crystallite size.

Regarding the residual stress measurement (i.e. for γ-phase (220)), it is found that sample AB exhibits tensile residual stresses of $79.1\,\mathrm{MPa} \pm$

Table 4. Determined surface roughness and mechanical properties.

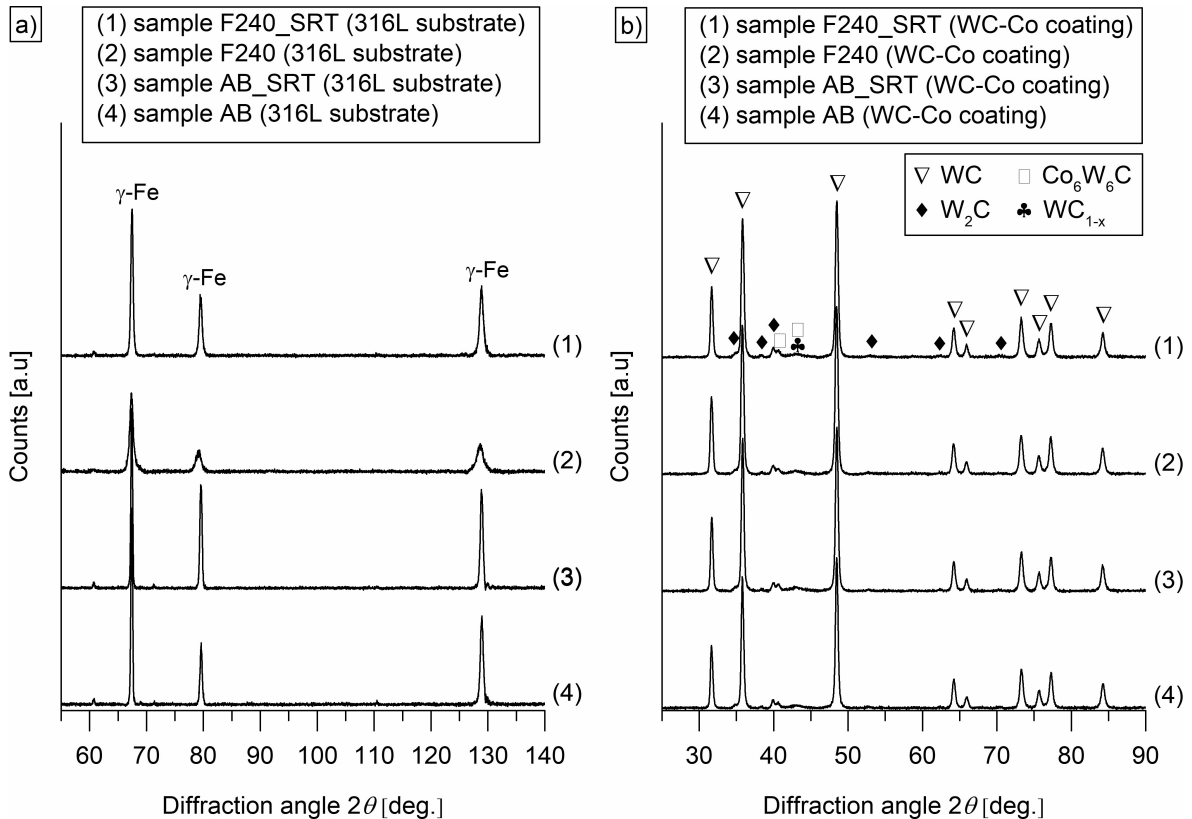| Sample	316 L substrate					tungsten carbide-cobalt coating
	R_a [µm]	R_z [µm]	$H_{s,center}$ [GPa]	$H_{s,interface}$ [GPa]	Residual stresses [MPa]	Residual stresses [MPa]
AB	9.8 ± 1.0	63.2 ± 5.8	2.98 ± 0.01	3.10 ± 0.02	79.1 ± 19.8	−1236 ± 54
AB_SRT	9.9 ± 2.1	66.1 ± 15.7	2.91 ± 0.02	2.96 ± 0.06	78.7 ± 16.4	−1526 ± 52
F240	7.3 ± 0,4	43.5 ± 3.0	3.02 ± 0.05	3.40 ± 0.09	−363.6 ± 16.8	−1341 ± 48.
F240_SRT	7.8 ± 1.8	45.3 ± 11.1	2.96 ± 0.03	3.20 ± 0.13	−29.4 ± 9.7	−1390 ± 75

Figure 1. X-ray diffraction patterns for the differently pre-treated 316 L substrates: a) non-heat-treated 316 L substrates, and b) 316 L substrates processed by SRT; the samples AS and AS/SRT serve as reference.

19.8 MPa, whereas sample F240 demonstrates compressive residual stresses of -363.6 MPa ± 16.8 MPa, Table 4. In contrast, the grit blasted and subsequent heat-treated substrate (sample F240_SRT) shows a significant reduction to -29.4 MPa ± 9.7 MPa. In terms of the as-built and subsequent heat-treated substrate (sample AB_SRT), the reduction in residual stresses is marginal (i.e. 78.7 MPa ± 16.4 MPa) and therefore negligible.

After thermal spraying, cross-section analyses of representative samples of composites (i.e. laser beam melting (LBM) substrate/high velocity oxy-fuel (HVOF) coating) confirm an all-side coating and reveal the absence of macroscopic defects such as cracks or delamination, *Figure 2*. With regard to the different composites, the light micrographs indicate a homogenous coating with a nearly constant coating thickness, as well as an adequate bonding to the differently pre-treated 316 L substrates.

As obtained from the nanoindentation experimentsthe 316 L substrate of sample AB shows a hardness $H_{s,center}$ of 2.98 GPa ± 0.01 GPa in the center, whereas the 316 L substrate near the sub-strate-coating interface demonstrates a hardness $H_{s,interface}$ of 3.10 GPa ± 0.02 GPa, Table 4. The heat-treated 316 L substrate of sample AB_SRT exhibits a $H_{s,center}$ of 2.91 GPa ± 0.02 GPa in the center, as well as a $H_{s,interface}$ of 2.96 GPa ± 0.05 GPa near the substrate-coating interface. In contrast, the 316 L substrate of sample F240 reveals a $H_{s,center}$ of 3.02 GPa ± 0.05 GPa in the center, whereas the 316 L substrate near the substrate-coating interface shows a $H_{s,interface}$ of 3.40 GPa ± 0.09 GPa. The same tendency is observed for the 316 L substrate of sample F240_SRT, demonstrating a $H_{s,center}$ and $H_{s,interface}$ of 2.96 GPa ± 0.03 GPa, and 3.20 GPa ± 0.13 GPa, respectively. It is found that the stress-relief heat treatment did not lead to any distinct change in hardness. The grit blasted 316 L sub-strates exhibit a higher hardness at the substrate-coating interface when compared to the hardness in the center, suggesting the introduction of strain hardening effects due to the impinging grit blasting particles. Moreover, the effectiveness of a peening effect caused by the impinging spray particles (i.e. hard particles) cannot be clearly demonstrated as
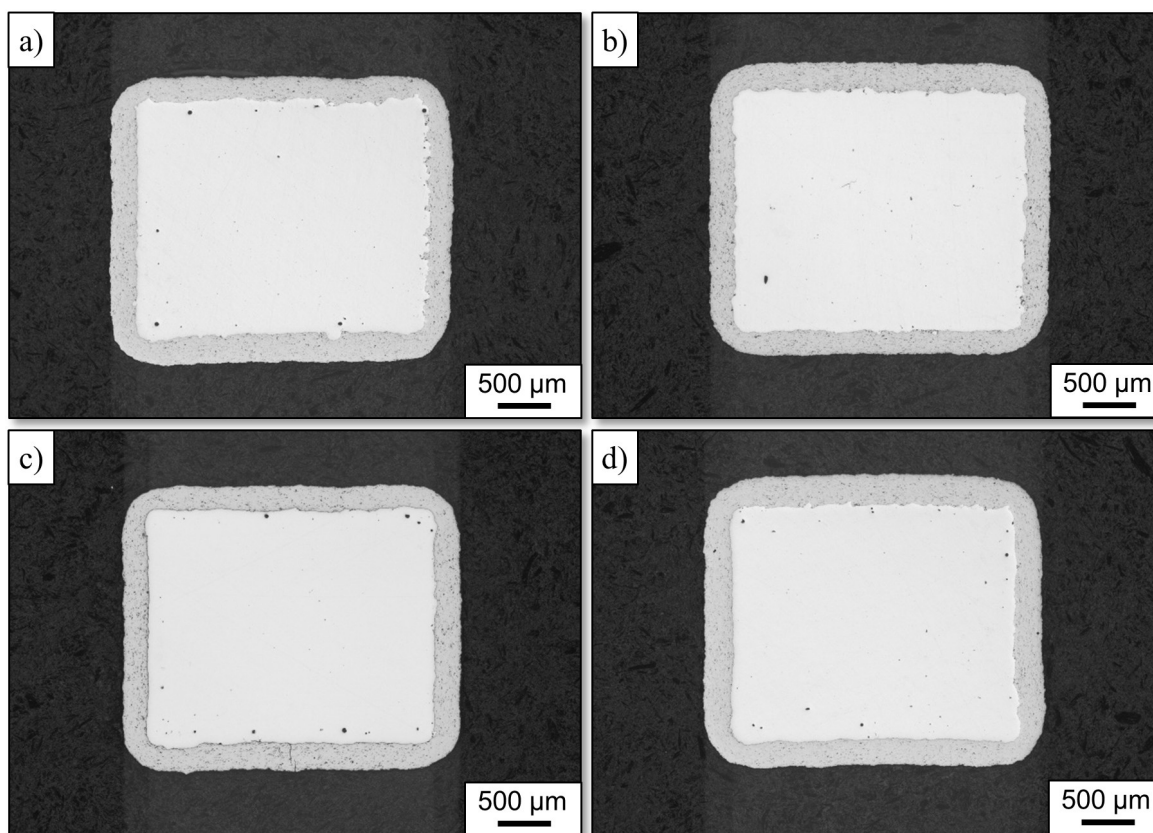
Figure 2. Cross-section images taken by light microscopy showing the high velocity oxy-fuel (HVOF) sprayed tungsten carbide-cobalt coating deposited onto differently pre-treated 316 L substrates: a) sample AB, b) sample AB_SRT, c) sample F240, and d) sample F240_SRT.

strain hardening effects are hardly evident, see nanoindentation near the substrate-coating interface for sample AB or AB_SRT, Table 4.

X-ray diffraction analyses of the tungsten carbide-cobalt coatings reveal that the deposits are mainly composed of hexagonal tungsten mono-carbide (WC), tungsten semi-carbide (W$_2$C), as well as traces of a non-stoichiometric cubic phase of tungsten carbide (WC$_{1-x}$) and eta carbide (Co$_6$W$_6$C), Figure 1b. The produced tungsten carbide-cobalt coatings of the different samples AB, AB_SRT, F240, and F240_SRT show no significant differences in phase composition. A distinct reflection of hexagonal or cubic cobalt cannot be found within the experimental resolution. In contrast, the tungsten carbide-cobalt feedstock (x-ray diffraction pattern not shown) consists of a mixture of hexagonal tungsten mono-carbide and cubic cobalt.

The residual stresses in the tungsten carbide-cobalt coating surface for sample AB, AB_SRT, F240, and F240_SRT were calculated for the (201)

reflection of hexagonal tungsten mono-carbide, Table 4. It is found that the tungsten carbide-cobalt coating deposited onto the differently pre-treated 316 L substrates exhibits compressive residual stresses in a range of -1236 MPa ± 54 MPa to -1526 MPa ± 52 MPa. A dependency on the different pre-treatments cannot be determined. Due to the strong momentum transfer by the impact of highly kinetic spray particles with a low melting degree (compared to other thermal spraying techniques), high velocity oxy-fuel (HVOF) sprayed tungsten carbide-cobalt coatings typically exhibit compressive residual stresses. However, the order of magnitude of residual stresses in this study is striking. The residual stress state, evolving in high velocity oxy-fuel (HVOF) sprayed coatings, depends mainly on the thermal conditions to which the substrate-coating system has been exposed [17]. Therefore, the final stress state can be assigned to a combination of quenching stresses, thermal stresses, and peening stresses. During cooling down to am-

bient temperature, thermal stresses develop due to the mismatch of thermal expansion between the coating and substrate. The resulting thermal stress is compressive if the coefficient of thermal expansion of the coating is lower than the coefficient of thermal expansion of the substrate material [18]. For a temperature range from 293 K to 1173 K, the coefficient of thermal expansion was demonstrated to be significantly lower for a high velocity oxy-fuel (HVOF) sprayed tungsten carbide-cobalt coating than compared to 316 L (i.e. bulk material) [19]. Therefore, it is assumed that thermal stresses make a substantial contribution to the compressive residual stress state in the tungsten carbide-cobalt coatings in this study. However, other effects such as tungsten carbide decomposition cannot be precluded.

As obtained from Vickers indentation tests, the tungsten carbide-cobalt coatings sprayed onto the differently pre-treated 316 L substrates show a fracture toughness K_{IC} of approximately 2.5 MPa $\sqrt{m} \pm$ 0.4 MPa $\sqrt{m}$. With regard to these results, it is obvious that the fracture toughness K_{IC} is remarkable low compared with either those observed for high velocity oxy-fuel (HVOF) sprayed tungsten carbide-cobalt coatings or tungsten carbide-cobalt ce-

mented carbides [20, 21]. The degree of decarburization in high velocity oxy-fuel (HVOF)-sprayed tungsten carbide-cobalt coatings has a decisive influence on the fracture toughness K_{IC} [22]. As reported by the authors, a decreased fracture toughness K_{IC} correlates with an increased decarburization. Based on the findings in this study, it is assumed that the decreased fracture toughness K_{IC} is caused by tungsten carbide decomposition phenomena and the embrittlement of the metallic binder phase.

The results of the low cycle fatigue tests of the different composites (i.e. laser beam melting (LBM) substrate/high velocity oxy-fuel (HVOF) coating) respect to the cycles to failure for various strain amplitudes, *Figure 3*. At a strain amplitude of 0.35 %, the mean lifetime of sample F240 and F240_SRT amounted to 1,325 and 1,294 cycles, respectively, as compared to 569 and 577 cycles for sample AB and AB_SRT, Figure 3a. Thus, the fatigue life of the laser beam melting (LBM) substrate/high velocity oxy-fuel (HVOF) coating composites with the use of the grit blasted substrates is slightly enhanced as compared to the use of substrates in their as-built condition. No significant differences (i.e. cycles to failure) can be observed
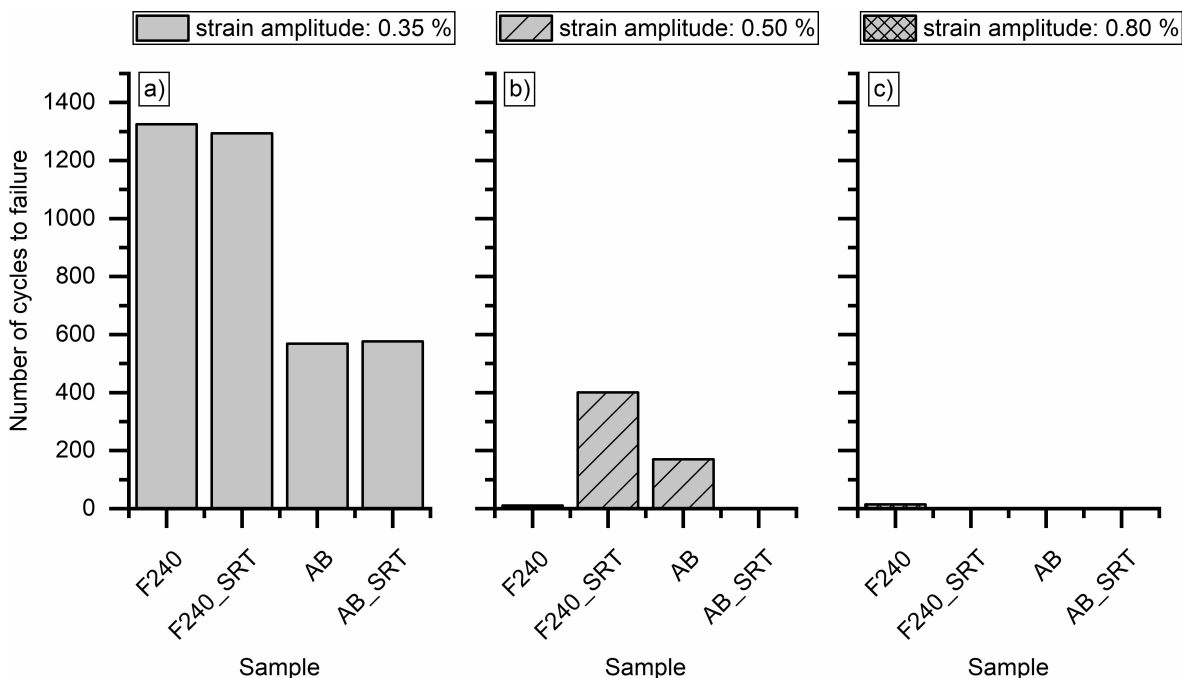

Figure 3. Cycles to failure for the different composites (i.e. laser beam melting (LBM) substrate/high velocity oxy-fuel (HVOF) coating) referring to as sample AB, AB_SRT, F240, F240_SRT: at a strain amplitude of a) 0.35 %, b) 0.50 %, and c) 0.80 %.

for the heat-treated samples. Thus, the stress-relief heat treatment does not lead to an increased low cycle fatigue strength. At higher strain amplitudes of 0.50 % and 0.80 %, the fatigue life dramatically decreases, Figure 3b, c. Accordingly, the samples mostly failed immediately. At a strain amplitude of 0.50 %, however, the mean lifetime of sample F240_SRT and AB amounted to 401 and 170 cycles, respectively.

The fracture surface morphologies were macroscopically analysed by means of optical microscopy, *Figures 4, 5*. After low cycle fatigue testing at high strain amplitudes (e.g. Figure 4, at a strain amplitude of 0.50 %), the macroscopic images illustrate serious surface damage, i.e. cracking, coating delamination and severe deformation of the composites. For the majority of samples, light micrographs of longitudinal-sections (i.e. perpendicular to the crack formation) reveal the evidence of cracks running through the 316 L substrate after the tungsten carbide-cobalt coating has been delaminated, for example sample AB_SRT, *Fig-*

*ure 6*a, b. Similar findings were observed after low cycle fatigue testing using a strain amplitude of 0.80 %.

At a strain amplitude of 0.35 %, the damage is less severe and shows a similar extent for all samples regardless of whether the 316 L substrates were grit blasted or heat-treated prior to the tungsten carbide-cobalt coating deposition. Accordingly, all samples show distinct crack formation in the tungsten carbide-cobalt coating, as well as the delamination of individual coating areas. The macroscopic fracture surface morphologies of samples F240 and AB_SRT after low cycle fatigue testing at a strain amplitude of 0.35 %, Figure 5. Longitudinal-sectional images suggest that crack initiation starts at the coating surface, for example sample AB_SRT, Figure 6c, d. The cracks propagate from their initiation sites through the coating towards the coating-substrate interface and finally penetrate the substrate. By comparing the hysteresis loops between sample F240 and AB_SRT at a strain amplitude of 0.35 %, it is demonstrated that
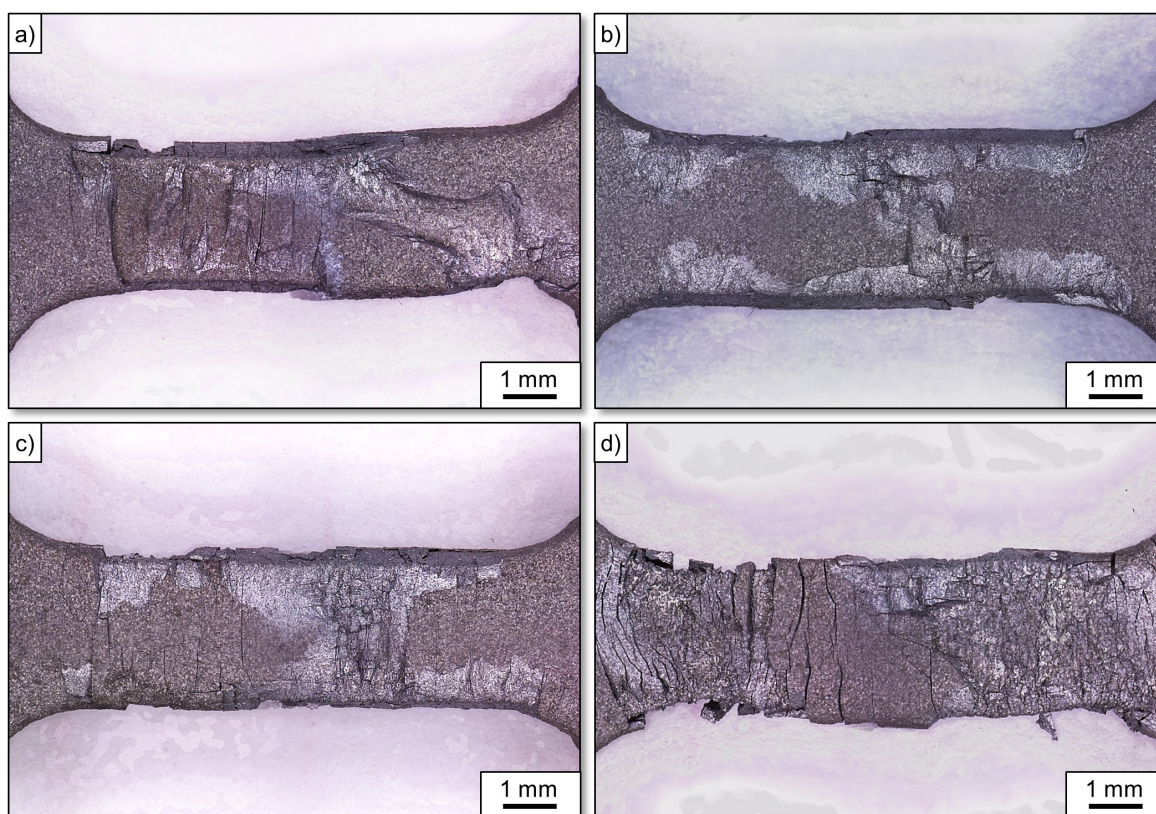

Figure 4. Optical micrographs showing the fracture surface morphologies after low cycle fatigue tests at a strain amplitude of 0.50 %: a) sample F240, b) sample F240_SRT, c) sample AB, and d) sample AB_SRT.
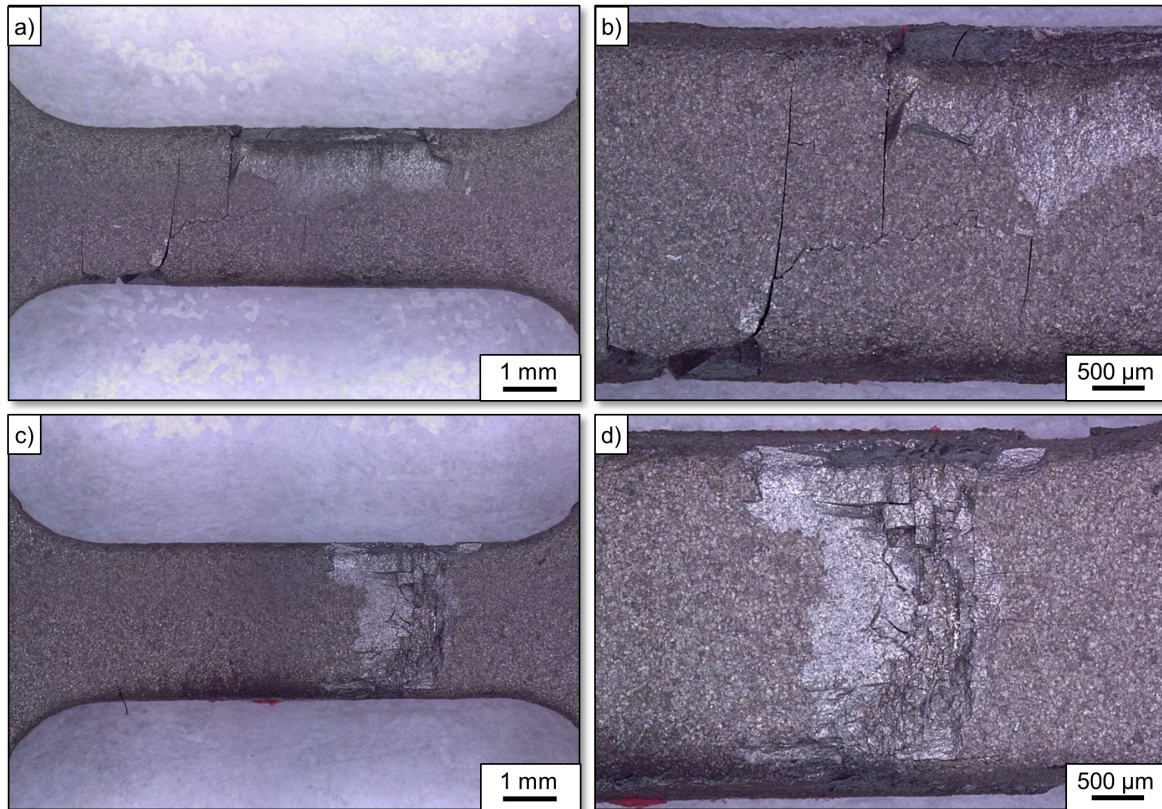
Figure 5. Optical micrographs showing the fracture surface morphologies after low cycle fatigue tests at a strain amplitude of 0.35 %: a) sample F240, b) enlarged view of sample F240, c) sample AB_SRT, and d) enlarged view of sample AB_SRT.

the AB_SRT curve shows only a small drop in force amplitude over the service life, *Figure 7*. In addition, no cracks can be detected, which allows the conclusion to be drawn that the coating fails, thus leading to a premature failure of sample AB_SRT. In contrast, the hysteresis loops of sample F240 demonstrate that a crack has been formed only after a certain time, suggesting that the sample fails later. It must be said that 3 % of the service life was chosen as starting value in order to represent the beginning of the service life and to minimize the influence of the settling of the machine.

With regard to the low cycle fatigue tests of the laser beam melting (LBM) substrate/high velocity oxy-fuel (HVOF) coating composites, fatigue cracking was predominantly initiated at the tungsten carbide-cobalt coating surface and propagated during cyclic loading through the coating towards the substrate-coating interface. Here, it is assumed that the cracks were nucleated near various heterogeneities of the tungsten carbide-cobalt coating surface. It is known that fatigue cracking can be miti-

gated by the introduction of surface compressive residual stresses. The insertion of compressive residual stresses in thermally sprayed coatings can lead to an increased fatigue life of the coated component [23]. Nevertheless, high residual stresses can cause fatigue failure, if their magnitude exceeds the yield strength of the coating material. Despite the high surface compressive residual stresses, the investigated tungsten carbide-cobalt coatings failed prematurely. The tungsten carbide-cobalt coatings were unable to plastically deform and demonstrated a brittle behavior. In this respect, the deposits showed a reduced fracture toughness K_{IC}, suggesting a poor crack resistance and breakage strength. Therefore, under the given experimental conditions, the fatigue life of the laser beam melting (LBM) substrate/high velocity oxy-fuel (HVOF) coating composites is largely determined by the fatigue behavior of the tungsten carbide-cobalt coating itself. For parts processed by laser beam melting (LBM), it is known that the process-related restrictions, such as residual stresses or sur-
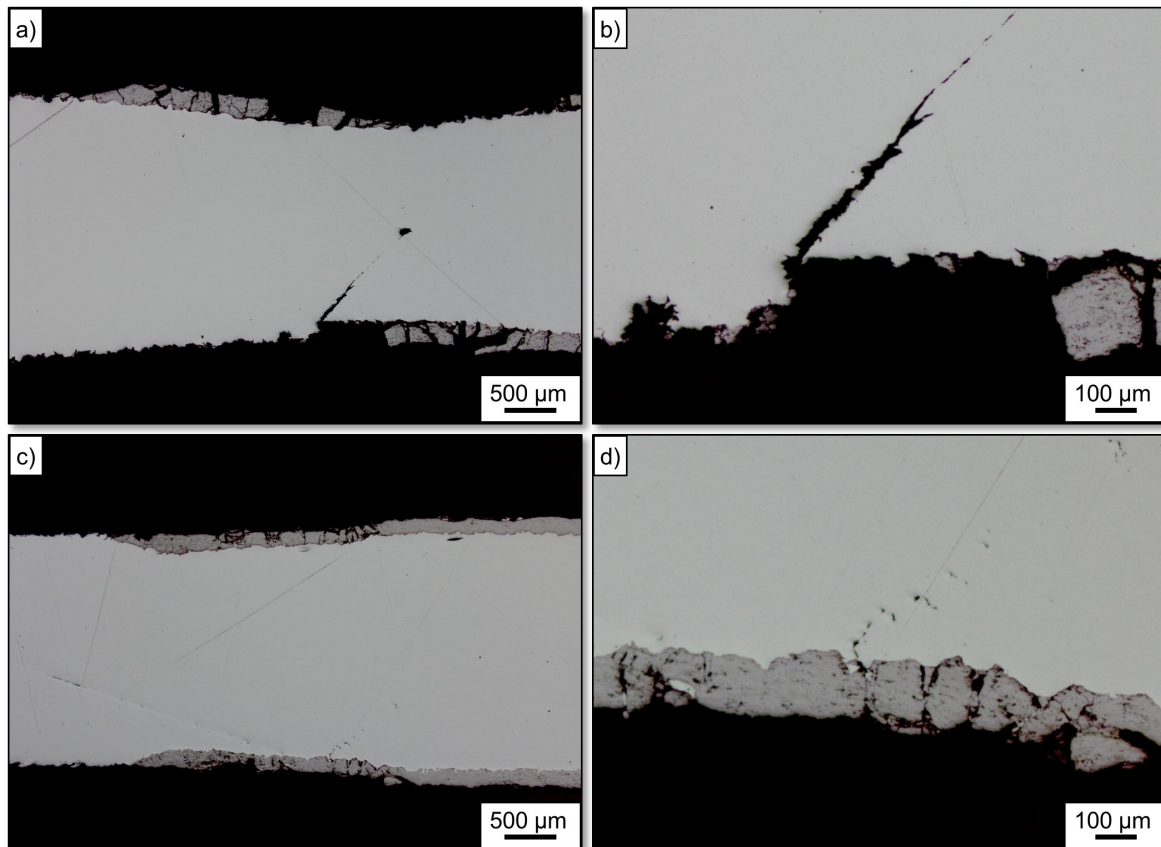
Figure 6. Optical micrographs showing the longitudinal-section of sample AB_SRT after low cycle fatigue tests: a, b) at a strain amplitude of 0.50 %, and c, d) at a strain amplitude of 0.35 %.

face roughness and porosity, have a substantial impact on the fatigue strength. Although the laser beam melting (LBM) substrate/high velocity oxyfuel (HVOF) coating composites with the use of grit blasted substrates showed improved fatigue behavior at low strain amplitudes, no clear correlation can be made in this study. In order to obtain a more precise correlation, further experiments of a larger number of samples at lower strain amplitudes such as 0.20 % should be carried out for the given material combination.

4 Conclusion

316 L substrates processed by laser beam melting (LBM) were subjected to different pre-treatment procedures prior to the deposition of a tungsten carbide-cobalt coating by means of high velocity oxyfuel (HVOF) spraying. Grit blasting the 316 L substrates led to the introduction of surface com-

pressive residual stresses, as well as strain hardening effects due to the impinging grit blasting particles. In addition, a subsequent stress-relief heat treatment of selected 316 L substrates resulted in a decline in residual stresses. Tungsten carbide-cobalt coatings were afterwards deposited onto the differently pre-treated 316 L substrates. Implementing low cycle fatigue tests at various strain amplitudes, the tungsten carbide-cobalt coated 316 L substrate composites demonstrated a poor fatigue strength since the tungsten carbide-cobalt coatings failed prematurely. The failure was predominantly attributed to crack initiation at the tungsten carbide-cobalt coating surface. X-ray diffraction analyses revealed that the tungsten carbide-cobalt coatings mainly consist of hexagonal tungsten mono-carbide, tungsten semi-carbide, as well as traces of a non-stoichiometric cubic phase of tungsten carbide and eta carbide. In addition, Vickers indentation tests indicated a reduced fracture toughness K_{IC}, resulting in a poor crack resistance and breakage
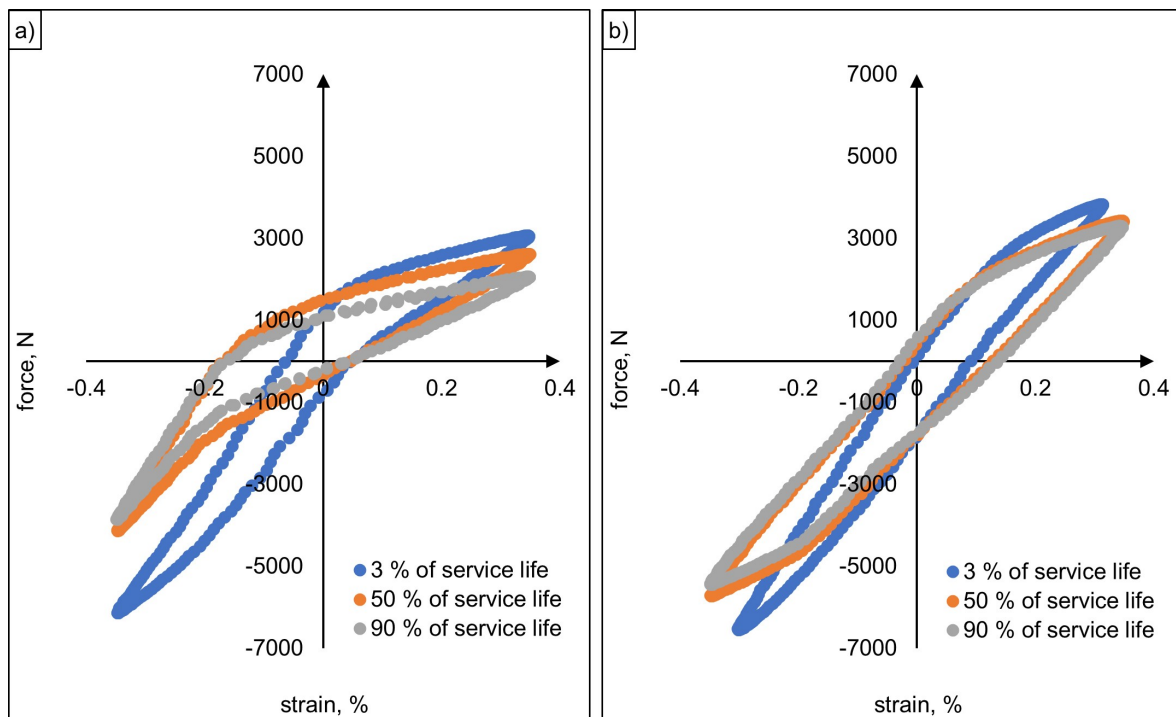
Figure 7. Hysteresis loops for the low cycle fatigue testing of different laser beam melting (LBM) substrate/high velocity oxy-fuel (HVOF) coating composites at a strain amplitude of 0.35 %: a) sample F240, and b) sample AB_SRT.

strength of the tungsten carbide-cobalt coatings. Therefore, the low cycle fatigue life of the laser beam melting (LBM) substrate/high velocity oxy-fuel (HVOF) coating composites was largely determined by the low cycle fatigue behavior of the tungsten carbide-cobalt coating itself. Despite the fact that the influence of the substrate pre-treatment on the resulting fatigue strength of the tungsten carbide-cobalt coated 316 L substrate composites was not clearly apparent, the low cycle fatigue tests also suggested that grit blasting the 316 L substrates prior to the coating deposition of tungsten carbide-cobalt led to an improved fatigue life of the composites.

Acknowledgements

5 References

[1] I. Gibson, D.W. Rosen, B. Stucker, *Additive Manufacturing Technologies, Springer US*, Boston, MA **2010**.

[2] S.A.M. Tofail, E.P. Koumoulos, A. Bandyopadhyay, S. Bose, L. O'Donoghue, C. Charitidis, *Mater. Today* **2018**, *21*, 22.

[3] H.A. Richard, B. Schramm, T. Zipsner, *Additive Fertigung von Bauteilen und Strukturen*, Springer Fachmedien Wiesbaden, Wiesbaden **2017**.

[4] J.-P. Kruth, M. Badrossamay, E. Yasa, J. Deckers, L. Thijs, J. Van Humbeeck, *in Proceedings of the 16th International Symposium on Electromachining*, Harmony Shanghai **2010**, pp. 1–12.

[5] Y. Liu, Y. Yang, D. Wang, *Int. J. Adv. Manuf. Technol.* **2016**, *87*, 647.

[6] J. Sander, *Ph.D. Thesis*, Technische Universität Dresden, Germany, **2017**.

[7] V.K.M. Karhu, *in 27th International Congress on Applications of Lasers and Electro-*

Optics, Laser Inst. of America, Orlando, Fla. **2008**, pp. 535–544.

[8] F. Brenne, *Ph.D. Thesis*, Universität Kassel, Germany, **2018**.

[9] K. Szymański, A. Hernas, G. Moskal, H. Myalska, *Surface and Coatings Technology* **2015**, *268*, 153.

[10] J.K.N. Murthy, D.S. Rao, B. Venkataraman, *Wear* **2001**, *249*, 592.

[11] Q. Yang, T. Senda, A. Ohmori, *Wear* **2003**, *254*, 23.

[12] A. Riemer, S. Leuders, M. Thöne, H.A. Richard, T. Tröster, T. Niendorf, *Engineering Fracture Mechanics* **2014**, *120*, 15.

[13] V. Hauk, H. Behnken, *Structural and residual stress analysis by nondestructive methods: Evaluation, application, assessment*, Elsevier, Amsterdam **1997**.

[14] B. Eigenmann, E. Macherauch, *Mat.-wiss. u. Werkstofftech.* **1995**, *26*, 199.

[15] W.C. Oliver, G.M. Pharr, *J. Mater. Res.* **1992**, *7*, 1564.

[16] D.K. Shetty, I.G. Wright, *J Mater Sci Lett* **1986**, *5*, 365.

[17] J. Stokes, L. Looney, *Surface and Coatings Technology* **2004**, *177*, 18.

[18] O.P. Oladijo, A.M. Venter, L.A. Cornish, N. Sacks, *Surface and Coatings Technology* **2012**, *206*, 4725.

[19] O. Sayman, F. Sen, E. Celik, Y. Arman, *Materials & Design* **2009**, *30*, 770; Design **2009**, 30, 770.

[20] N. Ma, L. Guo, Z. Cheng, H. Wu, F. Ye, K. Zhang, *Applied Surface Science* **2014**, *320*, 364.

[21] J.M. Tarragó, D. Coureaux, Y. Torres, E. Jiménez-Piqué, L. Schneider, J. Fair, L. Llanes, *International Journal of Refractory Metals and Hard Materials* **2018**, *71*, 221.

[22] P. Chivavibul, M. Watanabe, S. Kuroda, K. Shinoda, *Surface and Coatings Technology* **2007**, *202*, 509.

[23] J. Matejicek, S. Sampath, *Acta Materialia* **2001**, *49*, 1993.